Electronic Supplementary Information

High Performance Poly (methyl methacrylate) *via* Hindered Urea Bond Crosslinking

ShiWei Xie,[a] Dong Wang,[a] Sa Zhang,[a] JianHua Xu[b] and JiaJun Fu*[a]

a. School of Chemistry and Chemical Engineering, Nanjing University of Science & Technology, Nanjing 210094, P. R. China

b. Joint Laboratory of Advanced Biomedical Materials, College of Chemical Engineering, Nanjing Forestry University, Nanjing 210037, P. R. China

Table of Contents

Materials and Methods
Fig. S1 FTIR spectrum of PMMA, PMMA $Co_{0.1}$ and HUB-$C_{0.1}$ PMMA.
Fig. S2 ^{1}H NMR spectra of HUB-$C_{0.1}$ PMMA and *t*BAEMA
Fig. S3 ^{1}H NMR spectra of PMMA Co_x.
Fig. S4 GPC chromatograms of PMMA-Co_x with DMF as eluent.
Fig. S5 FTIR spectra of HUB-$C_{0.1}$ PMMA during crosslinking process.
Fig. S6 ^{13}C solid-state NMR spectra of PMMA, PMMA-$Co_{0.1}$, and HUB-$C_{0.1}$ PMMA.
Fig. S7 DSC curves of PMMA and PMMA Co_x.
Fig. S8 XRD curves of PMMA and HUB-C_x PMMA.
Fig. S9 TGA curves of PMMA and HUB-C_x PMMA.
Fig. S10 Relaxation process analysis of HUB-C_x PMMA.
Fig. S11 Dimensional illustration of dumbbell-shaped PMMA and HUB-C_x PMMA samples.
Fig. S12 Bending strain curves of PMMA and HUB-C_x PMMA.
Fig. S13 Optical photographs recording two HUB-$C_{0.1}$ PMMA samples being stretched.
Fig. S14 SEM image for the fracture surface of HUB-$C_{0.1}$ PMMA.
Fig. S15 Optical photographs for ball-drop test.
Fig. S16 Optical photographs for the dissolution of PMMA SL5000 samples in various solvents.
Fig. S17 Environmetal resistance of HUB-$C_{0.2}$ PMMA.
Fig. S18 Evolution of FTIR spectra of HUB-$C_{0.1}$ PMMA after being contacted with water molecule
Fig. S19 Creep-recovery plots for HUB-$C_{0.05}$ PMMA and HUB-$C_{0.2}$ PMMA under different temperatures.
Fig. S20. Normalized stress-relaxation curves of HUB-$C_{0.05}$ PMMA and HUB-$C_{0.1}$ PMMA.
Fig. S21 Arrhenius plots of HUB-C_x PMMA.
Fig. S22 Stress-relaxation curves of HUB-C_x PMMA at 80 °C.
Fig. S23 ATR-FTIR spectra of the original and the recycled HUB-$C_{0.1}$ PMMA.
Fig. S24 DSC curves of the original and the recycled HUB-$C_{0.1}$ PMMA.
Fig. S25 Temperature-dependence storage modulus of the original and the recycled HUB-$C_{0.1}$ PMMA.
Fig. S26 GPC chromatograms of original and recycled HUB-$C_{0.1}$ PMMA with DMF as eluent.
Fig. S27 Stress-relaxation curves of HUB-$C_{0.1}$ PMMA-C under different temperatures.
Fig. S28 Arrhenius plots of HUB-$C_{0.1}$ PMMA and HUB-$C_{0.1}$ PMMA-C.
Fig. S29 Stress-strain curves of the original and the recycled HUB-$C_{0.1}$ PMMA via liquid phase method.
Table S1 Mechanical properties of PMMA and HUB-C_x PMMA.
Table S2 Performance comparison
Reference
Movie S1. The demonstration for rapid crosslinking procedure for HUB-C_x PMMA.
Movie S2. The demonstration for the tensile stretching procedure of HUB-$C_{0.1}$ PMMA.
Movie S3. The demonstration for the sequential fracture of HUB-$C_{0.1}$ PMMA during stretching.
Movie S4. The demonstration for the performances of PMMA during ball drop impact test.
Movie S5. The demonstration for the performances of HUB-$C_{0.1}$ PMMA during ball drop impact test.
Movie S6. The demonstration for the performances of PMMA during SHPB test (v=10.6 m s^{-1}).
Movie S7. The demonstration for the performances of HUB-$C_{0.1}$ PMMA during SHPB test (v=10.6 m s^{-1}).

Materials and Methods

Materials

All chemicals were used as received without purification unless otherwise noted. Methyl methacrylate (MMA, ＞99.5%) and 2-(*tert*-butylamino) ethyl methacrylate (*t*BAEMA, ≥98%) were purchased from Macklin Reagent Co., Ltd., (Shanghai, China). MMA was passed through a column filled with basic alumina to remove inhibitors prior to polymerization. 2,2-Azobis(2-methyl propionitrile) (AIBN, 99%) was obtained from Sigma-Aldrich and recrystallized from methanol. Hexamethylene diisocyanate (HDI) was purchased from Aladdin Co., Ltd., (Shanghai, China). *N*,*N*-Dimethylformamide (DMF), Chloroform ($CHCl_3$) were dried with the molecular sieves for 24 h before use. Water used in all the experiments was obtained via a Milli-Q water system with a resistivity of 18.0 MΩ cm. Poly(methyl methacrylate) (PMMA SL5000, M_w～100,000 g mol^{-1}) homopolymer used for comparison was purchased from Degussa Co. (Germany).

Synthesis of PMMA Co_x

All PMMA Co_x (x=0.05, 0.1, and 0.2) in this work were synthesized via free radical solution polymerization using AIBN as the initiator and *t*BAEMA as the functional monomer. Typically, synthesis of PMMA-$Co_{0.1}$: AIBN (4.1 mg, 0.025 mmol), MMA (4.51 g, 45 mmol), *t*BAEMA (0.93 g, 5 mmol) and DMF (20 mL) were mixed in a 50 mL Schlenk tube, followed by stirring at room temperature for 20 minutes. After degassing by freeze-thaw over three cycles, the reactor was then immersed in an oil bath at 70 ˚C for 18 h. After reaction, the viscous solution was added dropwise into deionized water to precipitate and purify. Finally, the obtained product was allowed to dry for 48 h in a vacuum oven at 80 ˚C. The yield of the PMMA $Co_{0.1}$ (white bead) was determined to be approximately 90%. By changing the feed molar ratio, PMMA-$Co_{0.05}$ (AIBN: 4.1 mg, 0.025 mmol; MMA: 4.76 g, 47.5 mmol; *t*BAEMA: 0.46 g, 2.5 mmol) and PMMA-$Co_{0.2}$ (AIBN: 4.1 mg, 0.025 mmol; MMA: 4.0 g, 40 mmol; *t*BAEMA: 1.85 g, 10 mmol) could be prepared in the same method as that of PMMA-$Co_{0.1}$.

Synthesis of HUB-C_x PMMA

Typically, to synthesis of HUB-$C_{0.1}$ PMMA: The PMMA-$Co_{0.1}$ (1 g) was dissolved in 8 mL dry $CHCl_3$ in a 10 mL vial and a solution of the HDI crosslinker (74 μL, 0.46 mmol) in dry $CHCl_3$ (1 mL) was added. The mixed solution was poured into a polytetrafluorethylene (PTFE) mold and the solid was formed within 30 s. The resultant product was dried at room temperature under N_2 atmosphere for 12 h and under vacuum at 80 ˚C for another 48 h, yielding a transparent and colorless sheet. Clean and dry sheets were cut into small fragments and then compression molded into different shapes at 130 ˚C for 5 minutes under 0.5 MPa pressure. The HUB-$C_{0.05}$ PMMA (PMMA $Co_{0.05}$: 1g; HDI: 39 μL, 0.24 mmol) and HUB-$C_{0.2}$ PMMA (PMMA $Co_{0.2}$: 1 g; HDI: 137 μL, 0.85 mmol) samples were synthesized *via* the same method as that of HUB-$C_{0.1}$ PMMA, just changing molar ratio of PMMA-Co_x to HDI crosslinker. Please note that the molar ratio of HDI to *t*BAEMA in PMMA-$Co_{0.1}$ was fixed at 1:2.

Synthesis of HUB-$C_{0.1}$ PMMA-C: The PMMA-$Co_{0.2}$ (1 g) was dissolved in 8 mL dry $CHCl_3$ in a 10 mL vial and a solution of the HDI crosslinker (74 μL, 0.46 mmol) in dry $CHCl_3$ (1 mL) was added. Other procedures were consistent with that of HUB-$C_{0.1}$ PMMA.

Characterization

FTIR spectra were obtained using a Bruker Tensor 27 Fourier transform-infrared spectrometer equipped with attenuated total reflectance (ATR) in the range of 800-4000 cm^{-1}. The specimens were carefully pressed into a Specac Golden Gate MK II ATR for temperature-dependent FTIR tests and the corresponding data were performed 2D correlation analysis using the software 2D Shige version 1.3. ^{1}H NMR spectra were recorded on a Bruker DRX 500 NMR spectrometer using tetramethylsilane (TMS) as an internal reference at a room temperature. ^{13}C solid-state NMR spectrum were recorded on a Bruker AVANCE Ⅲ WB 400 MHz spectrometer. XRD measurements were performed on a Bruker D8 Advance using Cu Kα radiation (λ =0.1541 nm). The transparency tests were recorded by UV-vis spectrophotometer (Thermo Fisher E220), and the spectra were collected over a range from 400 nm to 800 nm. The molecular weight and dispersity were evaluated by GPC (Waters 1515) using DMF as the eluent, and narrowly dispersed PMMA species were employed as standard. The glass transition temperature (T_g) was determined by a differential scanning calorimetry (TA DSC-25), which was performed from -20 ˚C to 200 ˚C at a 10 ˚C min^{-1} under nitrogen flow. TGA experiments were conducted on a Mettler 851e at heating rate of 10 ˚C min^{-1} under nitrogen atmosphere in the temperature range of 50 to 600 ˚C. Optical microscope images were recorded by Jiangnan MV3000 optical microscope. SEM were conducted on a Hitachi S-4800 field emission electron microscope. High-speed video camera (Phantom V710) was used to capture the momentary states of samples during ball-drop experiments (YCLC-134 drop ball tester, YuHan Mechanical Co. Ltd., Shanghai, China). In SHPB experiments, the diameter of all the aluminum bars were 14.5 mm. The length of the transmitter, strike and incident bars were 2000, 200, and 1500 mm, respectively. The static contact angles were measured using an autosampler (3.0 μL volume of deionized water) by the Optical Contact Angle & interface tension meter-SL200KS (USA KINO Industry Co., Ltd.). Fluorescence microscopy images were performed on a Jiangnan BM2000 fluorescence microscope. Dynamic vapour sorption (DVS) was tested by a TA VTI-SA Vapor sorption analyzer.

Mechanical tests

Uniaxial tensile tests were conducted on dumbbell-shaped samples (ISO 527-2 type 5B) using a Shimadzu AGS-X tester under the following conditions: room temperature (25 ˚C), a humidity of 50%, a strain rate of 1.5 mm min^{-1}, and a gauge length of 10 mm. At least three times of each sample were tested, and the average value was given. The loading-unloading were obtained under the same conditions. The Young's modulus was calculated as the initial slope of the tensile curves. DMA measurements were performed on a TA Q800 instruments, and the temperature dependency storage modulus curves were obtained using a single cantilever clamp. The rectangular-shaped samples (length of 35 mm, width of 13.5 mm, thickness of 1 mm) were heated from 30 ˚C to 180 ˚C at a heating rate of 5 ˚C min^{-1} with a constant frequency of 1 Hz. DMA tests were also used in

tensile creep resistance experiments at 80 ˚C, each rectangular-shaped sample (length of 5 mm, width of 3 mm, thickness of 0.2 mm) was subjected to a constant stress of 1 MPa for 10 minutes using tensile clamp. Bending modulus was also performed on DMA with a bending rate of 1.5 mm min^{-1} using three-point bending clamp. The rheological experiments were tested on a TA AG R2 rheometer equipped with a 20-mm-diameter parallel steel plate. Stress relaxation experiments were performed at a constant strain of 1% in the temperature range from 120 to 160 ˚C. Creep-recovery experiments were carried out by exerting a constant stress of 1 kPa for 1000 seconds and subsequently releasing it for 1000 seconds to recovery.

Dissolution experiments

The rectangular-shaped samples (length: 13.5 mm, width: 8.5 mm, thickness: 1 mm) of approximately 125 mg were immersed in 20 mL various solvents, including *N*,*N*-dimethylformamide (DMF), dimethyl sulfoxide (DMSO), ethanol (EtOH), tetrahydrofuran (THF), acetonitrile (ACN), 1,4-dioxane (Diox), methanol (MeOH), ethyl acetate (EA) and acetone (DMK) at 25 ˚C for 24 h. Then, the samples were dried at 100 ˚C for 48 h to the constant weight (M_2). The weight of the initial sample was signed as M_0. The weight of the sample immediately taken out from solvent was expressed as M_1. The swelling ratio (*SR*) and soluble fraction (*SF*) were calculated according to the equations: $SR = (M_1 - M_0)/M_0$; $SF = 1 - M_2/M_0$.

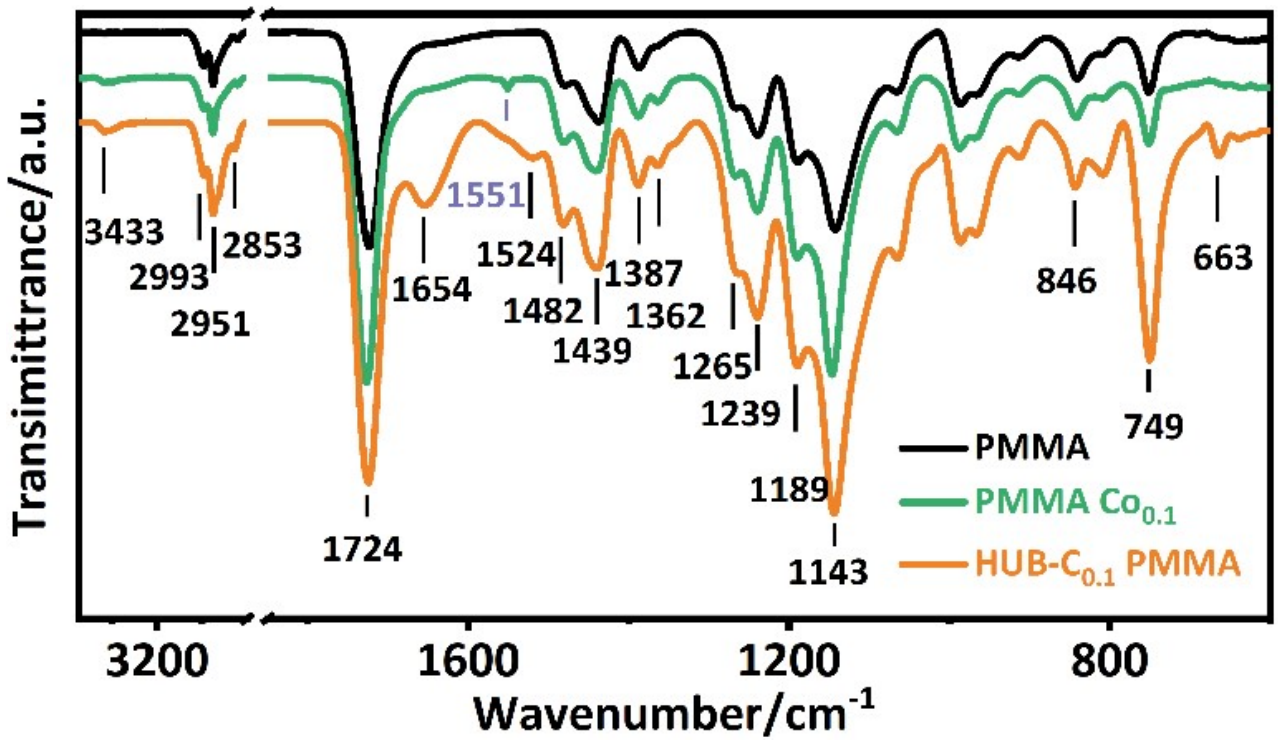

Fig. S1 FTIR spectrum of PMMA, PMMA $Co_{0.1}$ and HUB-$C_{0.1}$ PMMA.

FTIR (cm^{-1}): 3433 (-NH stretching vibration), 2993/2951 (-CH_3 and -CH_2- asymmetric stretching vibration), 2853 (-CH_3 symmetric stretching vibration), 1724 (C=O stretching vibration of ester), 1654 (C=O stretching vibration of urea), 1551/1524 (-NH bending vibration), 1482(-CH_2- scissoring vibration), 1439(-CH_2- asymmetric deformation vibration), 1387 (-O-CH_3 deformation vibration), 1362 (-$C(CH_3)_3$ stretching vibration), 1265/1239 (-C-O-C- asymmetric stretching vibration), 1189/1143 (C-O-C symmetric stretching vibration), 846 (-C-C- skeleton vibration), 749 (-CH_2- wagging vibration) and 663 (-$(CH_2)_3$- bending vibration).

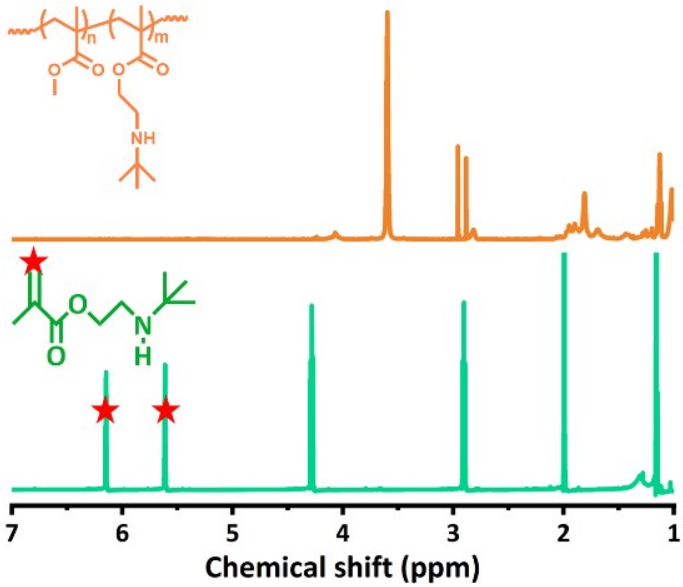

Fig. S2 ^1H NMR spectra of PMMA $Co_{0.1}$ and *t*BAEMA (500 MHz, $CDCl_3$, 25 °C).

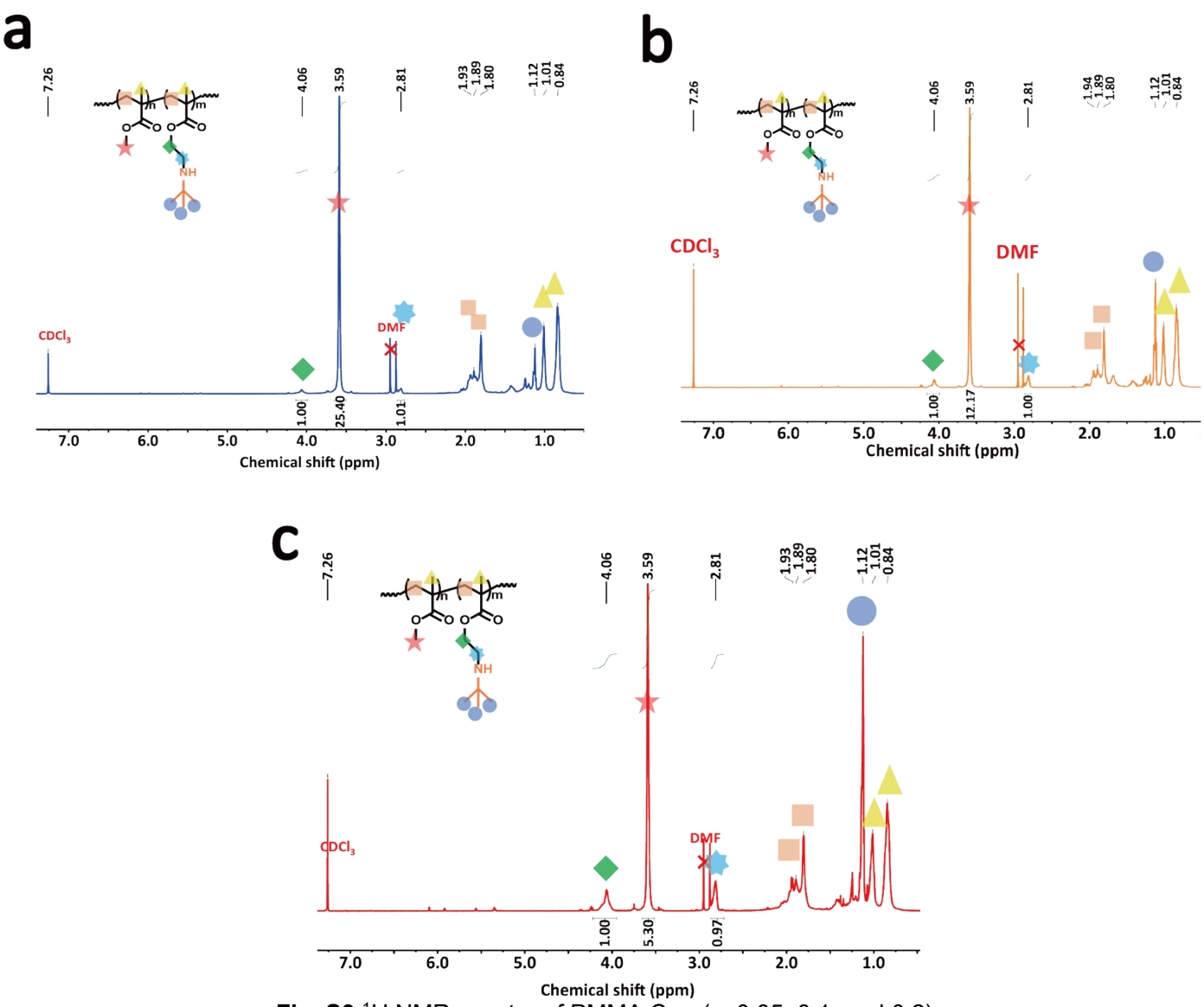

Fig. S3 ^{1}H NMR spectra of PMMA Co_x. (x=0.05, 0.1, and 0.2)

Based on the analysis of ^{1}H NMR spectra, molar ratio of *t*BAEMA to comonomer was determined.

As for PMMA $Co_{0.05}$, A_x refers to the area of the signal in Figure S2a,

% *t*BAEMA= $\{((A_{blue+green})\times 2) / [(A_{blue+green}) \times 2 + (A_{yellow}) \times 3]\} \times 100\%$

% *t*BAEMA= $[(2.01\times 2) / (2.01\times 2 + 25.4\times 3)] \times 100\% = 5.01\%$

As for PMMA $Co_{0.1}$, A_x refers to the area of the signal in Figure S2b,

% *t*BAEMA= $\{((A_{blue+green}) \times 2) / [(A_{blue+green}) \times 2 + (A_{yellow}) \times 3]\} * 100\%$

% *t*BAEMA= $[(1.00\times 2) / (1.00\times 2 + 12.17\times 3)] \times 100\% = 9.87\%$

As for PMMA $Co_{0.2}$, A_x refers to the area of the signal in Figure S2c,

% *t*BAEMA= $\{((A_{blue+green}) \times 2) / [(A_{blue+green}) \times 2 + (A_{yellow}) \times 3]\} \times 100\%$

% *t*BAEMA= $[(1.00\times 2) / (0.97\times 2 + 5.30\times 3)] \times 100\% = 19.9\%$

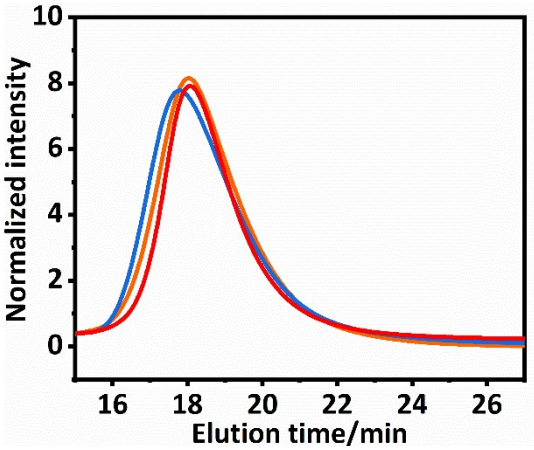

Fig. S4 GPC chromatograms of PMMA-Co_x (x=0.05, 0.1, and 0.2) with DMF as eluent.

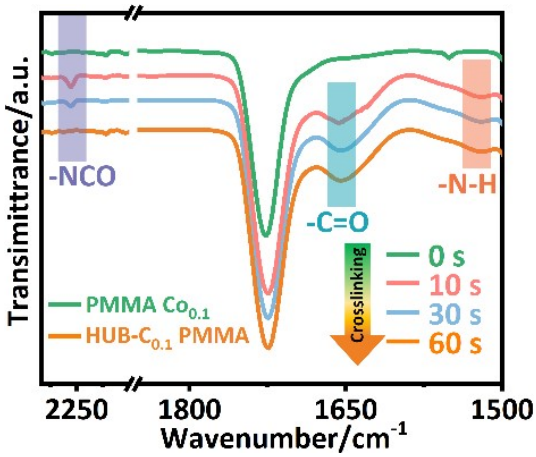

Fig. S5 FTIR spectra of HUB-$C_{0.1}$ PMMA during crosslinking process.

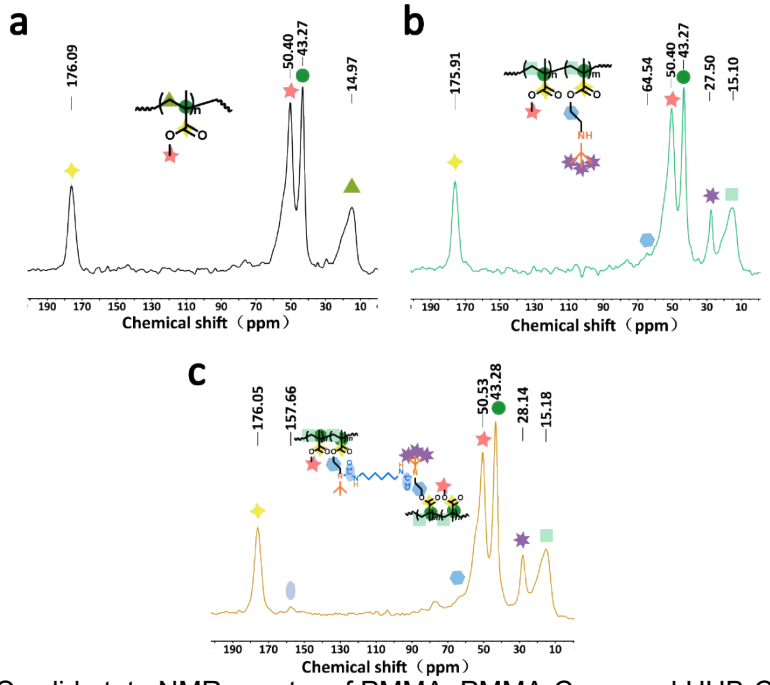

Fig. S6 ^{13}C solid-state NMR spectra of PMMA, PMMA-$Co_{0.1}$, and HUB-$C_{0.1}$ PMMA.

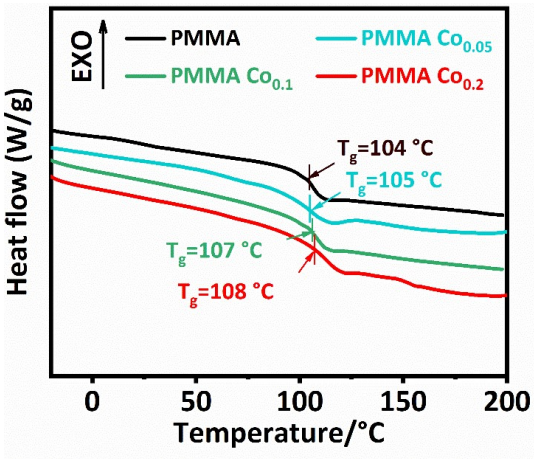

Fig. S7 DSC curves of PMMA and PMMA Co_x. (x=0.05, 0.1, and 0.2)

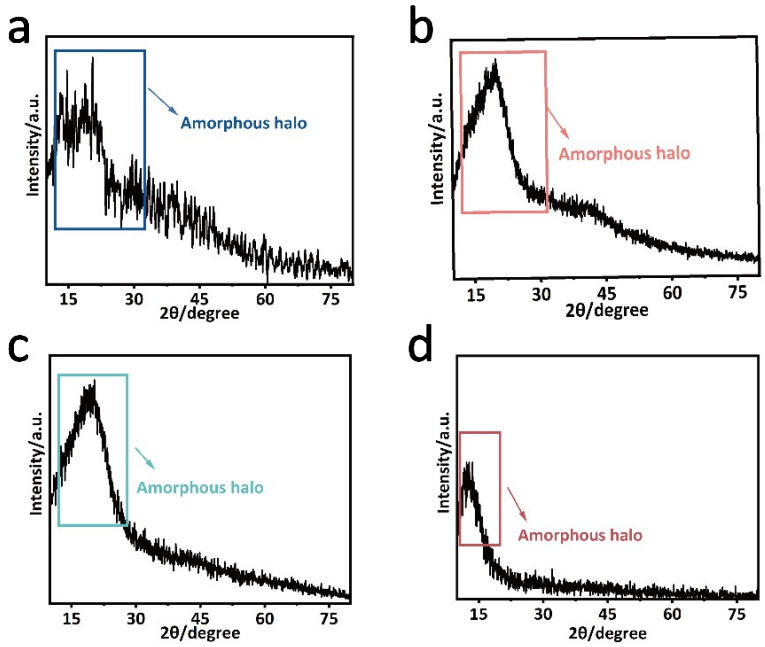

Fig. S8 XRD curves of PMMA and HUB-C_x PMMA. (x=0.05, 0.1, and 0.2)

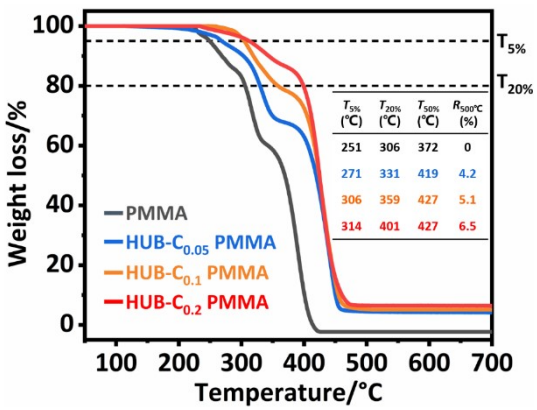

Fig. S9 TGA curves of PMMA and HUB-C_x PMMA. (x=0.05, 0.1, and 0.2)

$T_{5\%}$, $T_{20\%}$ and $T_{50\%}$ represent thermal decomposition temperature at 5%, 20%, and 50% weight loss. $R_{500°C}$ represents the residue weight at 500 °C.

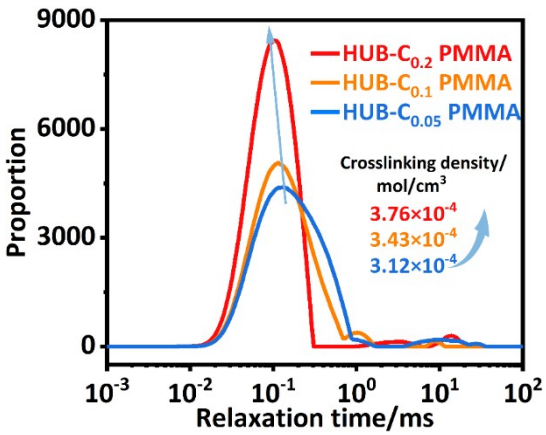

Fig. S10 Relaxation process analysis of HUB-$C_{0.05}$ PMMA，HUB-$C_{0.1}$ PMMA and HUB-$C_{0.2}$ PMMA.

As shown in Fig. S10, the relaxation time decreased with increase in molar ratio of *t*BAEMA. The crosslinking densities of HUB-$C_{0.05}$ PMMA, HUB-$C_{0.1}$ PMMA, and HUB-$C_{0.2}$ PMMA are 3.12×10^{-4}, 3.43×10^{-4}, and 3.76×10^{-4} mol cm^{-3}, respectively, which is also in line with expectations.

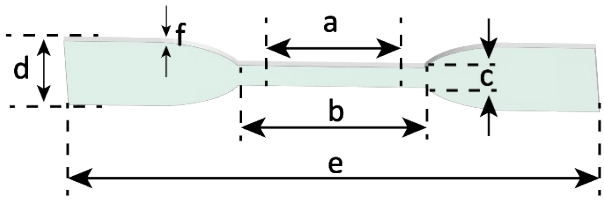

Sample specimen used in tests:

a: 10 mm (gauge length)
b: 12 mm
c: 2 mm
d: 6 mm
e: 35 mm
f: 1-1.2 mm

Fig. S11 Dimensional illustration of dumbbell-shaped PMMA and HUB-C_x PMMA samples. (x=0.05, 0.1, and 0.2)

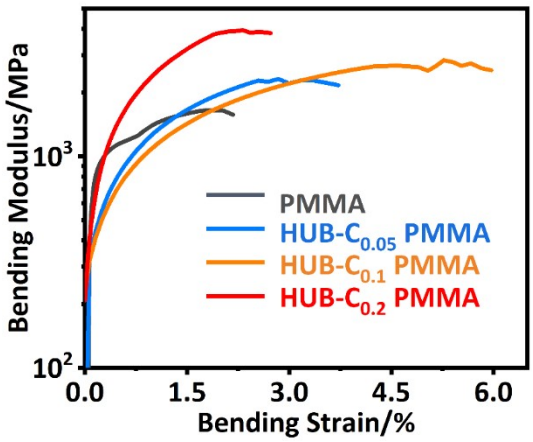

Fig. S12 Bending stress-strain curves of PMMA and HUB-C_x PMMA. (x=0.05, 0.1, and 0.2)

According to equation S1, bending modulus can be calculated.

$$E = \frac{3}{2}\frac{Fl}{\lambda b h^2} \qquad \text{(equation S1)}$$

Where *E* is bending modulus, *F* is load, *l* is length of clamping, *b* is width of specimen, *h* is height of sample, and *λ* is bending strain.

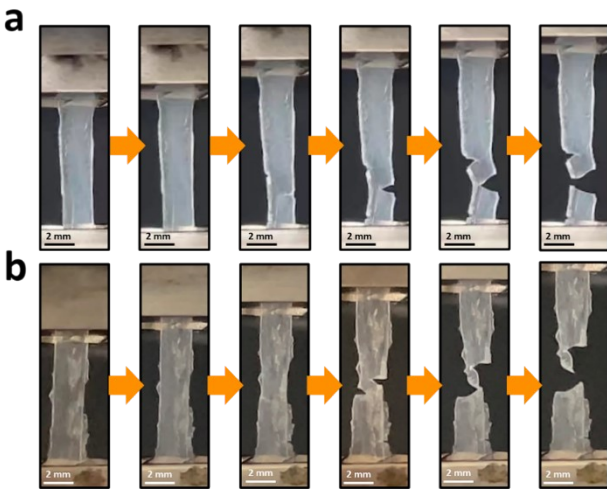

Fig. S13 Optical photographs recording two HUB-$C_{0.1}$ PMMA samples being stretched.

As can be seen from Fig. S10, the original carack terminated, and the new cracks appeared and continued to propagate to dissipate energy.

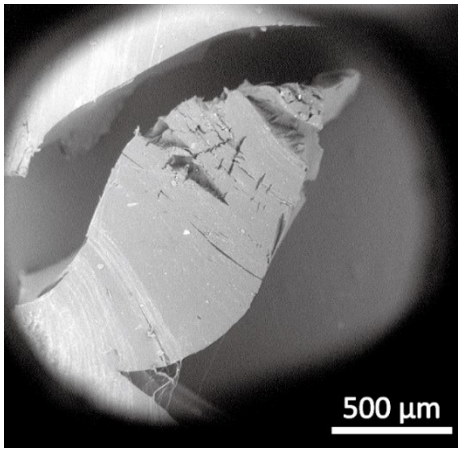

Fig. S14 SEM image for the fracture surface of HUB-$C_{0.1}$ PMMA.

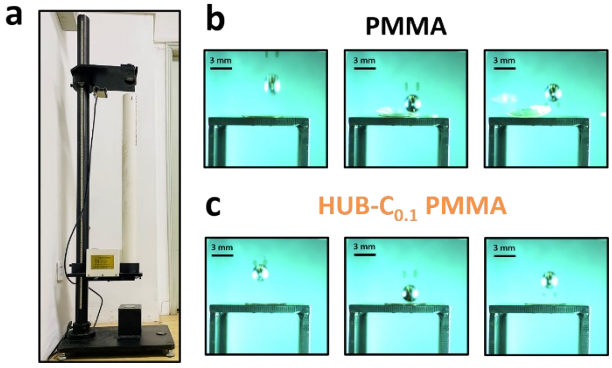

Fig. S15 a) Optical photograph for ball-drop test. Frames taken by a high-speed camera showing the impact of metal ball on PMMA sample b) and HUB-$C_{0.1}$ PMMA sample c).

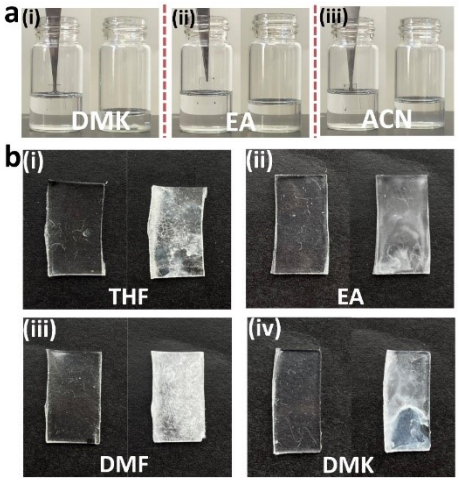

Fig. S16 a) Optical photographs for the dissolution of PMMA SL5000 samples in i) DMK, ii) EA, and iii) ACN within 6h under ambient conditions. b) Optical photographs for PMMA SL5000 samples before and after soaking in i) THF, ii) EA, iii) DMF, and iv) DMK at 25 °C for 3 min.

Fig. S17 a) Swelling ratio, soluble fraction and gel fraction of HUB-$C_{0.1}$ PMMA and b) HUB-$C_{0.2}$ PMMA in various solvents at 25 °C for 24 h. c) Creep resistance at 80 °C of HUB-$C_{0.1}$ PMMA and HUB-$C_{0.2}$ PMMA samples (5 × 3 × 0.2 mm). d) Tensile curves for PMMA and HUB-C_x PMMA (x=0.05, 0.1, 0.2, 0.25). It can be easily seen from Fig. S17, the higher molar ratio of *t*BAEMA, the better solvent resistances. Both HUB-$C_{0.2}$ PMMA and HUB-$C_{0.25}$ PMMA show the feature of brittle fracture. Although the modulus, tensile strength, and environmental resistance are all enhanced as increase in molar ratio of *t*BAEMA, the weakness of toughness threatens the safe use of HUB-$C_{0.2}$ PMMA and HUB-$C_{0.25}$ PMMA.

a

Solvent	Swelling ratio	Soluble fraction (%)	Gel fraction (%)
Diox	0.01	1.3	98.7
ACN	0	2.1	97.9
EA	0	2.1	97.9
EtOH	0.09	0.7	99.3
DMK	0	2.3	97.7
MeOH	0.13	0.8	99.2
DMF	0.13	0	100
THF	0.07	1.7	98.3
DMSO	0.01	2.3	97.7

b

Solvent	Swelling ratio	Soluble fraction (%)	Gel fraction (%)
Diox	0.01	0.7	99.3
ACN	0	0.7	99.3
EA	0	0	100
EtOH	0.09	0	100
DMK	0	2.0	98.0
MeOH	0.13	0.7	99.3
DMF	0.13	0	100
THF	0.07	1.5	98.5
DMSO	0.01	2.1	97.9

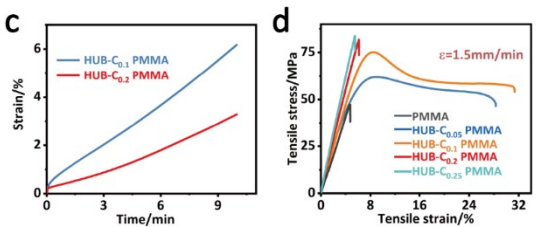

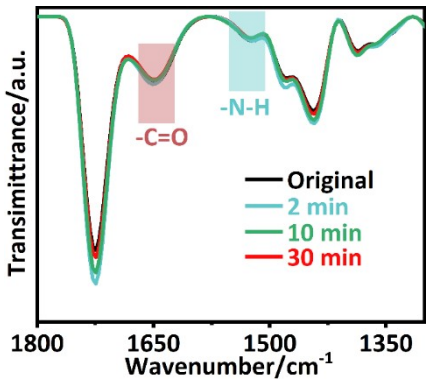

Fig. S18 Evolution of FTIR spectra of HUB-$C_{0.1}$ PMMA after being contacted with water molecule.

As shown in Fig. S18, after being contacted with water, the locations of -NH- (1551 cm^{-1}) and -C=O (1654 cm^{-1}) did not change, proving that water molecules cannot form hydrogen bonds with amide groups (-NH-, -C=O) within HUB-$C_{0.1}$ PMMA. This is the main reason for the low water absorption and the ability for maintaining mechanical properties under high humidity.

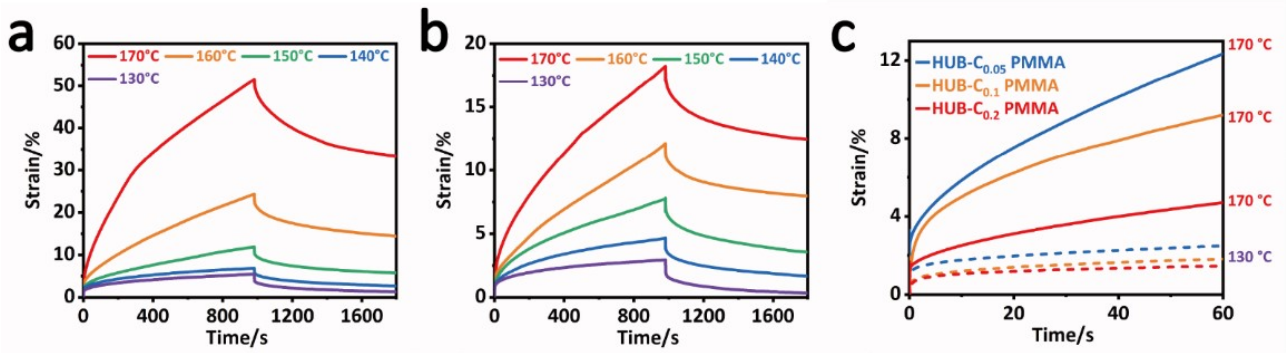

Fig. S19 Creep-recovery plots for HUB-$C_{0.05}$ PMMA a) and HUB-$C_{0.2}$ PMMA under different temperatures. c) Creep-recovery plots for HUB-C_x PMMA on the elastic region (σ = 1000 Pa) at 170 °C and 130 °C.

Viscosities and relaxation time were extracted from the linear regimes of the creep-recovery plots using the equation S2 and equation S3:

$$\eta = \frac{\sigma}{\gamma} \qquad \text{(equation S2)}$$

where η is viscosity, σ is constant stress (1000 Pa), and γ is strain rate (determined from the slope of the linear fit).

$$\tau = \eta J_{eq} \qquad \text{(equation S3)}$$

where τ is relaxation time, η is viscosity, J_{eq} is Shear creep compliance (determined from the intercept of the linear fit)

130 ˚C: η=1.1×10^7 Pa.s and τ=122.4 s for HUB-$C_{0.05}$ PMMA, η=1.5×10^7 Pa.s and τ=153.1 s for HUB-$C_{0.1}$ PMMA, η= 1.8×10^7 Pa.s and τ= 174.1 s for HUB-$C_{0.2}$ PMMA.

170 ˚C: η= 5.3×10^5 Pa.s and τ= 17.7 s for HUB-$C_{0.05}$ PMMA, η= 9.4×10^5 Pa.s and τ= 26.6 s for HUB-$C_{0.1}$ PMMA, η= 1.7×10^6 Pa.s and τ= 34.5 s for HUB-$C_{0.2}$ PMMA.

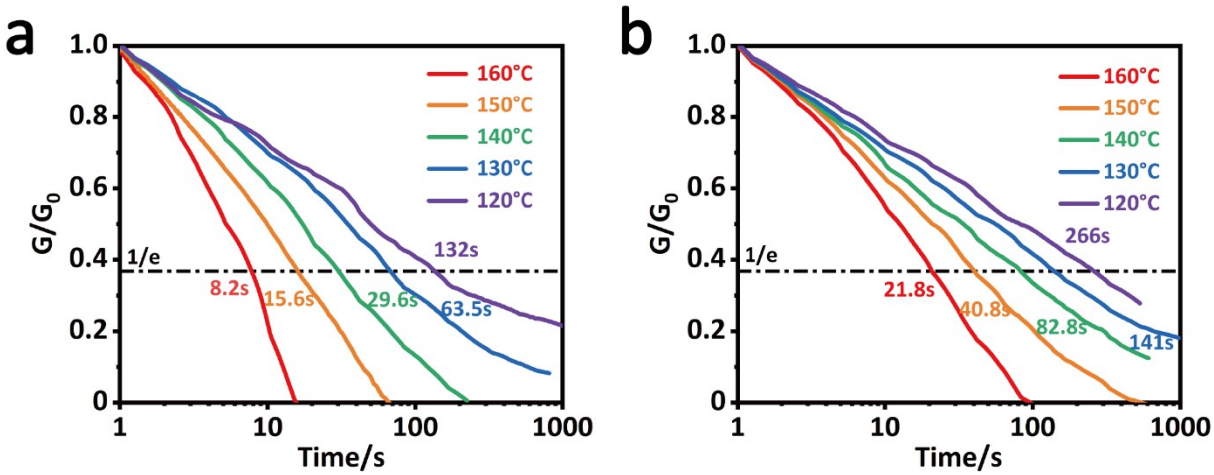

Fig. S20 Normalized stress-relaxation curves of HUB-$C_{0.05}$ PMMA a) and HUB-$C_{0.2}$ PMMA b).

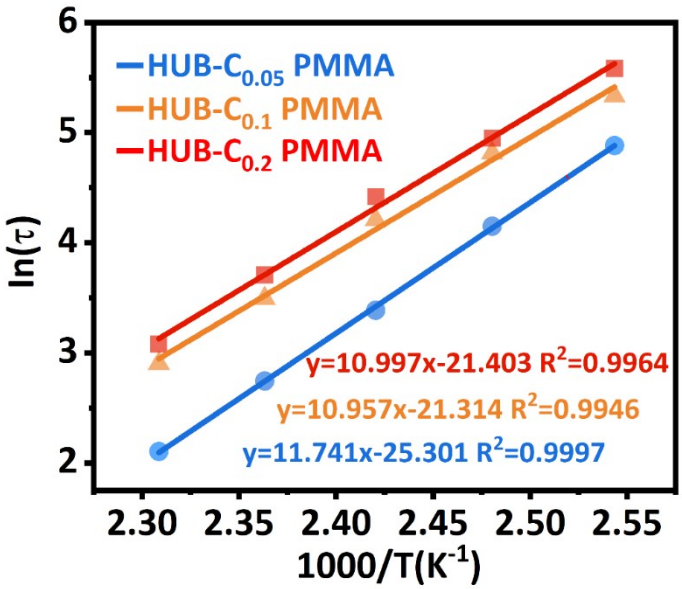

Fig. S21 Arrhenius plots of HUB-C_x PMMA. (x=0.05, 0.1, and 0.2)

The activation energy (E_a) of HUB-C_x PMMA were calculated using equation S4.

$$ln(\tau) = \frac{E_a}{RT} + In(\tau_0) \qquad \text{(equation S4)}$$

τ is relaxation time, R is ideal gas constant (8.314 J mol^{-1} K^{-1}), T is temperature.

According to Figure S16, E_a/R is 11.74 for HUB-$C_{0.05}$ PMMA, E_a/R is 10.9 for HUB-$C_{0.1}$ PMMA, and E_a/R is 11 for HUB-$C_{0.2}$ PMMA. Therefore, the activation energy of HUB-$C_{0.05}$ PMMA, HUB-$C_{0.1}$ PMMA and HUB-$C_{0.2}$ PMMA are calculated to be 97.5, 91.1 and 91.5 kJ mol^{-1}, respectively.

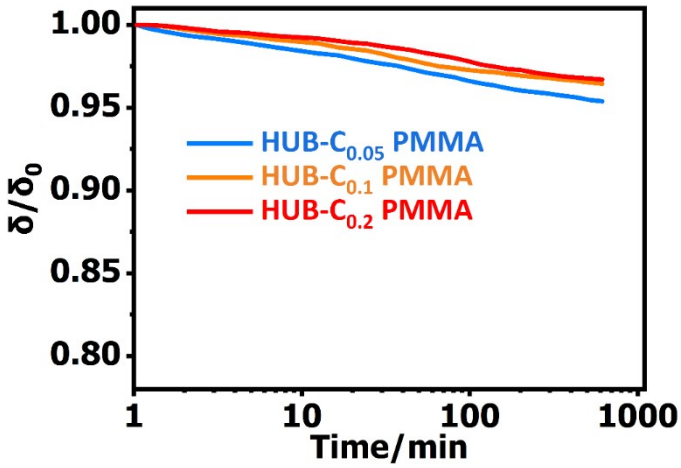

Fig. S22 Stress-relaxation curves of HUB-C_x PMMA at 80 °C. (x=0.05, 0.1, and 0.2)

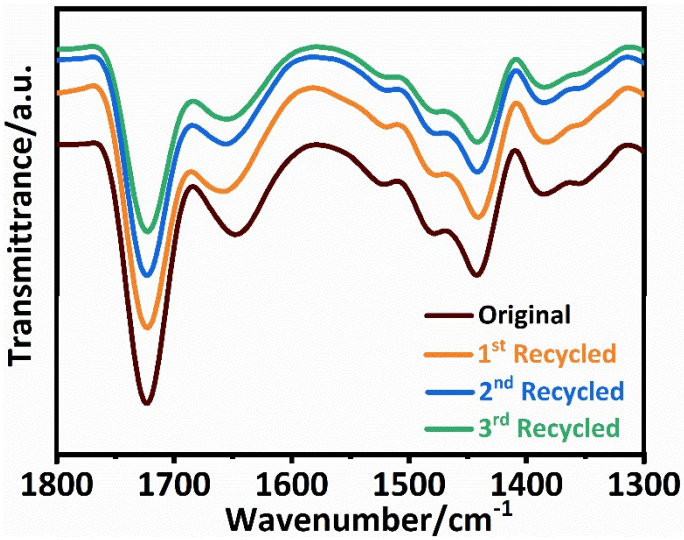

Fig. S23 ATR-FTIR spectra of the original and the recycled HUB-$C_{0.1}$ PMMA.

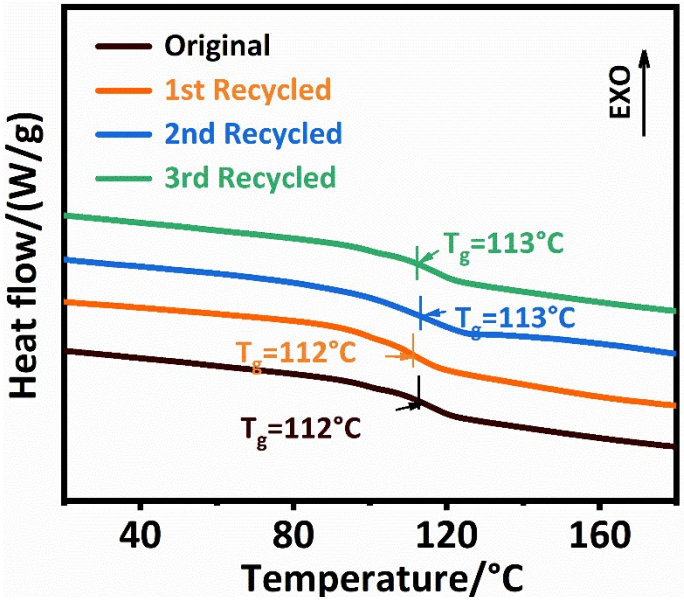

Fig. S24 DSC curves of the original and the recycled HUB-$C_{0.1}$ PMMA.

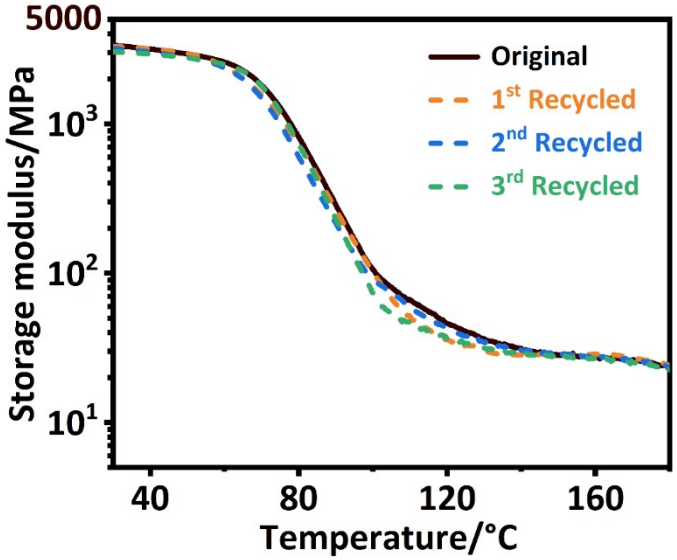

Fig. S25 Temperature-dependence storage modulus of the original and the recycled HUB-$C_{0.1}$ PMMA.

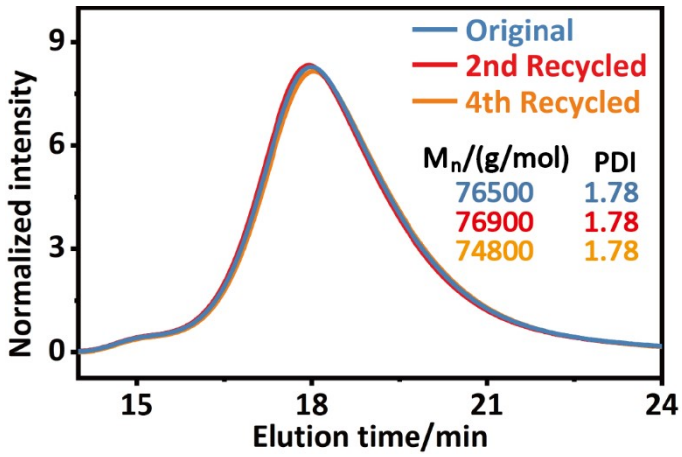

Fig. S26 GPC chromatograms of original and recycled HUB-$C_{0.1}$ PMMA with DMF as eluent.

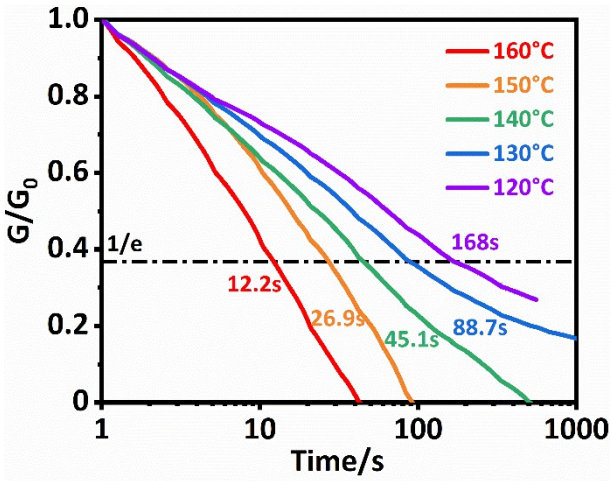

Fig. S27 Stress-relaxation curves of HUB-$C_{0.1}$ PMMA-C under different temperatures.

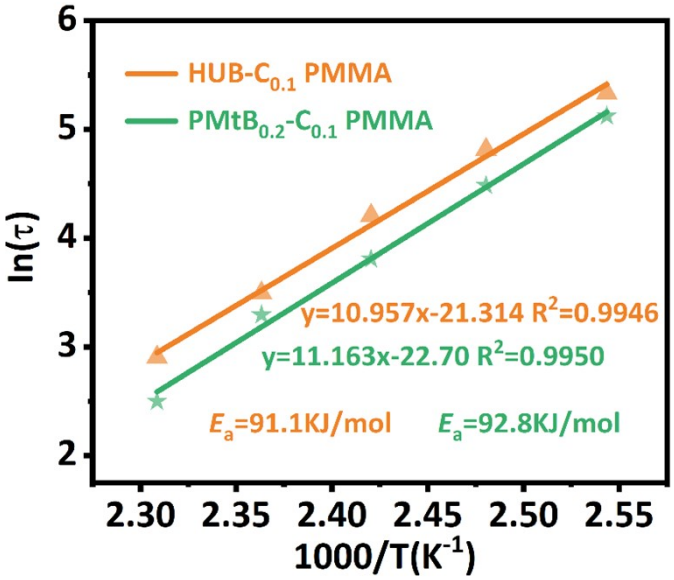

Fig. S28 Arrhenius plots of HUB-$C_{0.1}$ PMMA and HUB-$C_{0.1}$ PMMA-C.

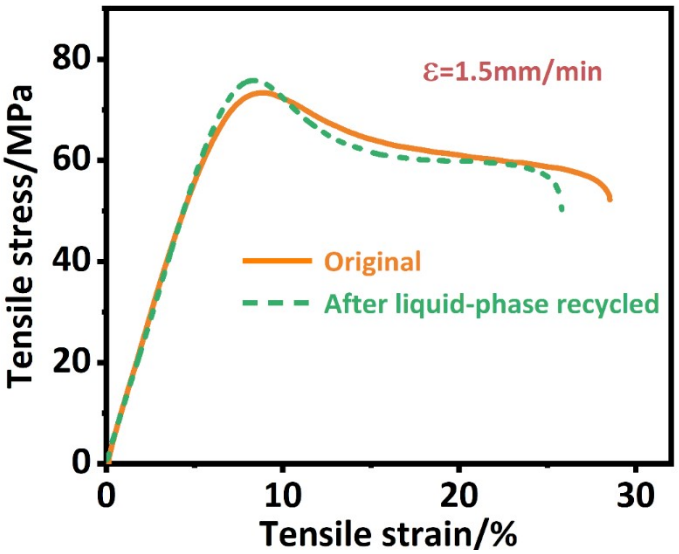

Fig. S29. Stress-strain curves of the original and the recycled HUB-$C_{0.1}$ PMMA via liquid phase method.

Table S1 Mechanical properties of PMMA and HUB-C_x PMMA. (x=0.05, 0.1, and 0.2)

Samples	Young's modulus (MPa)	tensile strength (MPa)	elongation at break (%)	toughness (MJ/m^3)
PMMA	973 ± 39.5	46.2 ± 1.92	4.80 ± 0.32	0.85 ± 0.27
HUB-$C_{0.05}$ PMMA	1343 ± 46.8	60.2 ± 1.09	26.1 ± 1.90	10.2 ± 1.13
HUB-$C_{0.1}$ PMMA	1396 ± 39.9	76.5 ± 0.43	28.8 ± 2.54	13.4 ± 1.39
HUB-$C_{0.2}$ PMMA	1478 ± 61.6	82.0 ± 2.16	5.90 ± 0.86	3.37 ± 0.56

Table S2. Performance comparisons of HUB-$C_{0.1}$ PMMA with other modified PMMA reported in the previous literatures

Sample	Method	Improvement in Young's modulus	Improvement in tensile strength	Improvement in fracture strain	Improvement in toughness	Appearance	Ref.
PMMA-CNF composite fibers (CNF content 3 wt%)	Cellulose nanofibrils reinforcement	1.35×	1.19×	1.21×	1.55×	Not mentioned	S1
PLA/PB-g-SAN/PMMA (45/ 30/25)	PLA/PB-g-SAN/PMMA ternary blends	0.58×	0.57×	21.80×	25.60×	White	S2
PMMA/Particle Brushes (PB content 7wt%)	Fillers (SiO_2-g-(PBA-b-PSAN) particle brushes)	0.98×	1.09×	1.36×	1.69×	Loss of transmittance	S3
PMMA/GPMMA (GPMMA content 0.5wt%)	Solvent exfoliated graphene reinforcement	2.50×	2.15×	1.99×	5.69×	Loss of transmittance	S4
15% TiO2-PMMA nanocomposite	Nano TiO_2 reinforcement	1.95×	1.62×	Not mentioned	1.02×	Not mentioned	S5
CP50(2.9% nanofibers volume fraction)	(PAN/PMMA) core–shell nanofibers	1.42×	1.26×	0.68×	0.98×	Loss of transmittance	S6
P (MMA-co-MAA-co-SPMA) Copolymer (87.4/10/0.6)	Copolymerization	1.07×	1.33×	0.89×	1.18×	Colorless and transparent	S7
PMMA V3(120 kg/mol)	Dioxaborolane metathesis crosslinking	0.99×	1.03×	Not mentioned	Not mentioned	Colorless and transparent	S8
PMMA vitrimer	Vinylogous urethane crosslinking	1.03×	1.01×	Not mentioned	Not mentioned	Yellow	S9
PMMA V3	Dioxaborolane metathesis crosslinking	1.48×	1.73×	1.15×	Not mentioned	Not mentioned	S10
HUB-$C_{0.1}$ PMMA	Hindered urea bond crosslinking	1.43×	1.66×	4.00×	15.70×	Colorless and transparent	This work

Reference

[S1] S. V. Gnana, K. Ethan, M. L. Lisa, V. Nikhil, M. C. Craig, M. C. John, T. T. Kevin, *ACS Appl. Polym. Mater.*, 2021, **3**, 6102-6110.

[S2] M. M. Mazidi, A. Edalat, R. Berahman, F. S. Hosseini, *Macromolecules*, 2018, **51**, 4298-4314.

[S3] J. M. Kubiak, J. J. Yan, J. Pietrasik, K. Matyjaszewski, *Polymer*, 2017, **117**, 48-53.

[S4] J. Wang, Z. Shi, Y. Ge, Y. Wang, J. Fan, J. Yin, *Mater. Chem. Phys.*, 2012. **136**, 43-50.

[S5] A. Chatterjee, *J. Appl. Polym. Sci.*, 2010, **118**, 2890-2897.

[S6] S. Borhani, A. Zadhoush, *M. Fathi, J. Appl. Polym. Sci.*, 2020, **137**, 49192.

[S7] S. Chen, C. Xu, M. Ma, Y. Shi, H. He, K. Yuan, R. Xu, X. Wang, *Polym. Adv. Tech.*, 2021, **32**, 1230-1238.

[S8] M. Rottger, T. Domenech, R. Weegen, A. Breuillac, R, Nicolay, L. Leibler, *Science*, 2017, **356**, 62-65.

[S9] J. J. Lessard, L. F. Garcia, C. P. Easterling, M. B. Sims, K. C. Bentz, S. Arencibia, D. A. Savin, B. S. Sumerlin, *Macromolecules*, 2019, **52**, 2105-2111.

[S10] Z. Wang, Y. Gu, M. Ma, M. Chen, *Macromolecules*, 2020, **53**, 956-964.